Formation of iron-rich phyllosilicates in the FeO-SiO_2-H_2O system during hydrothermal synthesis as a function of pH

Liva Dzene[a,*], Amira Doggaz[a], Patrick Dutournié[a], Sayako Inoué[b], Mustapha Abdelmoula[c], Alexandra Jourdain[a], Jean-Marc Le Meins[a], Jocelyne Brendlé[a], Christelle Martin[d], Nicolas Michau[d]

[a] Institut de Science des Matériaux de Mulhouse CNRS UMR 7361, Université de Haute-Alsace, Université de Strasbourg, 3b rue Alfred Werner, 68093 Mulhouse CEDEX, France

[b] Geodynamics Research Center (GRC), Ehime University, 2-5 Bunkyo-cho, Matsuyama, Ehime 790-8577, Japan

[c] LCPME, CNRS-Université de Lorraine UMR7564, 54000 Nancy, France

[d] Andra, Scientific & Technical Division, Waste, Radionuclides, Chemicals & Geochemistry Department, 1/7 rue Jean Monnet, F-92298 Châtenay-Malabry CEDEX, France

*liva.dzene@uha.fr

Submitted : 3 November 2023. Revised 10 March 2024. Associate Editor Javier Huertas

ABSTRACT

The formation of iron-rich phyllosilicates can occur at different natural or engineered settings. In this study, the influence of pH for the hydrothermal synthesis of iron-rich phyllosilicates was investigated in the range from 8.50 to 12.10 with respect to the pH after the aging of the precursor. The synthesized samples were characterized by powder X-ray diffraction, Raman and Mössbauer spectroscopies, and transmission electron microscopy. Three domains of pH were identified, and correlated with the silica availability and its speciation in the solution. The formation of 1:1 type Fe^{III}/Fe^{II} phyllosilicate was observed between pH 9.67 and 10.75. Above pH=10.75 two types of phyllosilicate-like mineral phases were observed. In addition to 1:1 type Fe^{III}/Fe^{II} phyllosilicate, 2:1 type Fe^{III}/Fe^{II} phyllosilicate was observed. Below pH=9.67, mainly

This is a 'preproof' accepted article for Clay Minerals. This version may be subject to change during the production process.
DOI: 10.1180/clm.2024.8

amorphous silica and iron oxides were observed. The findings showed that pH governed crystallinity and nature of obtained phyllosilicate-like phases.

Keywords: hydrothermal synthesis, iron-rich phyllosilicates, solubility of silica, serpentine, tri-octahedral

Highlights:

- pH determines the nature of the synthesized iron-rich phase, i.e. 2:1 or 1:1 type.
- Silica availability depends on the dissolution rate (driven by pH) and changes the molar ratio Fe/Si, influencing the type of phyllosilicate obtained.

Introduction

The damage of materials due to corrosion or scale formation can occur in engineered systems, especially when silicon and iron species are present in aqueous solution. Such conditions might occur (1) in fluid conducting pipes in brine handling equipment, and (2) on glass-steel-cement interfaces in the context of nuclear waste repository. In hyper-saline brines, the solution is basic, and a high concentration of silica and iron can occur leading to the precipitation of Fe-rich phyllosilicates (Manceau, 1995). The scale formation can then clog pipes and damage other equipments. In the context of nuclear waste repository, the pH of cement material surrounding steel containers is basic. As a result, some dissolved silica is expected to be present if the material is wet and porous. In contact with metal where some Fe(II) could be leached, the formation of phyllosilicates can then be promoted leading to further corrosion of steel (Lanson *et al.*, 2012; Herbert *et al.*, 2016). For the vitrified nuclear waste, Si-OH species are present on the glass surface in significant amounts. In contact with steel and dissolved Fe(II), phyllosilicate precipitation can thus be expected due to a high Si:Fe ratio, as shown in the studies of Carriere *et al.* (2021) and Galai *et al.* (2023), which identified phyllosilicate phases at the glass-steel interface. Silica consumption can induce glass alteration and, in some cases, accelerate the degradation of materials. The environmental conditions (element aqueous concentrations, pH, redox potential) of the formation of iron-rich layered phyllosilicates in the FeO-SiO_2-H_2O system are poorly understood. Therefore, the synthesis in laboratory can bring new insight in this field.

https://doi.org/10.1180/clm.2024.8 Published online by Cambridge University Press

Synthesis of iron-rich phyllosilicates using different protocols have been well documented (Petit *et al.*, 2017; Dzene *et al.*, 2018). The hydrothermal path remains the preferred one because of its versatility and the ease of use which allows obtaining relatively well crystallized products (Kloprogge, 1998; Jaber *et al.*, 2013). Many parameters having influence on synthesis products, such as synthesis time and temperature, chemical composition and pH have been studied over time (Kloprogge, 1994; Lantenois *et al.*, 2005; Tosca *et al.*, 2016; Boumaiza *et al.*, 2020). For example, the preparation of precursor using Fe^{2+} could enhance the kinetic of synthesis and the crystallinity of the product (Decarreau & Bonnin, 1986). In general, it was also reported that low temperatures (below 150°C) and short synthesis time favor the formation of Fe-serpentines (1:1 type phyllosilicate) whereas higher temperature (above 200°C) and longer synthesis time lead to the formation of Fe-rich saponite or chlorite (2:1 type phyllosilicate) (Grubb, 1971; Bertoldi *et al.*, 2005; Mosser-Ruck *et al.*, 2010; Pignatelli *et al.*, 2014; Boumaiza *et al.*, 2020).

Among the different enlisted synthesis parameters above, it has been demonstrated that pH had the most impact on the nature of phases formed (Cundy & Cox, 2005; Baron *et al.*, 2016; Tosca *et al.*, 2016; Boumaiza *et al.*, 2020). Indeed, the quantity of hydroxyl anions (OH^-) in solution determines the speciation of elements and the solubility of reactants and products. Regarding the speciation of elements as a function of pH, Frank-Kamenetzkij *et al.* (1973) concluded in their study that for the mineral transformations which go through the dissolution and precipitation, the pH of the medium controls the speciation of Al and thus the coordination of Al (octahedral vs tetrahedral) in newly formed structures. In a former study, de Kimpe *et al.* (1961) reported the formation of zeolite (where Al is tetrahedrally coordinated) in basic pH, and kaolinite (where Al is octahedrally coordinated) in acidic pH. In addition, the recent study of Criouet *et al.* (2023) demonstrated the influence of the amount of OH^- for the synthesis of clay minerals. For the same chemical composition of the reactants, kaolinite was obtained in solution with pH below 12, beidellite (with both, octahedrally and tetrahedrally coordinated Al) was obtained with a solution at pH=12, and zeolites (with only tetrahedrally coordinated Al) were formed in solutions with pH above 12. In alkaline pH, it has also been shown that the crystal chemistry of Fe(III)-nontronites is heavily controlled by the aqueous Si speciation, which is pH-dependent (Baron *et al.*, 2016). An increase in the proportion of $H_2SiO_4^{2-}{}_{(aq)}$ over $H_3SiO_4^-{}_{(aq)}$ was shown to enhance the Fe(III)-Si substitution in the obtained nontronites.

Regarding the FeO-SiO_2-H_2O system, Francisco *et al.* (2020) demonstrated that polymerization of $Fe(OH)_2$ occurred at basic pH, whereas the precipitation of amorphous SiO_2 was observed

https://doi.org/10.1180/clm.2024.8 Published online by Cambridge University Press

below pH 8, inhibiting the polymerization of $Fe(OH)_2$. In addition, the studies of Schwertmann & Thalmann (1976) and Doelsch *et al.* (2002) demonstrated the formation of Si-O-Fe(II) bonds at basic pH, hindering the polymerization of Fe(II) compounds. Halevy *et al.* (2017) observed the formation of green rust-like compounds at neutral pH, and the formation of iron-rich phyllosilicate (greenalite-like) phases at basic pH was observed in the presence of silica (Konhauser *et al.*, 2007; Tosca *et al.*, 2016; Hinz *et al.*, 2021).

In our previous study, we observed that for the same targeted chemical composition, a high amount of hydroxyl ions available in the solution favored the precipitation of 2:1 type phyllosilicate with respect to 1:1 type phyllosilicate whereas small quantity of OH^- favored the formation of 1:1 type phyllosilicate (Boumaiza *et al.*, 2020). Given the strong dependence of type of clay mineral obtained in function of pH, and the pH dependence of silicon and iron species and/or compounds speciation and solubility, the aim of this work was then to go a step further and investigate if a definite pH value can be found for the precipitation of 1:1 type iron-rich phyllosilicate in the FeO-SiO_2-H_2O system. As mentioned above, the environmental conditions of the formation of iron-rich layered phyllosilicates, in particular those of 1:1 type phyllosilicates, in the FeO-SiO_2-H_2O system are not well-known. The lack of such knowledge then leads to the degradation of materials and decreases the durability of engineered systems where the formation of such phases can occur. An improved understanding about the formation mechanisms of these phases would allow to prevent their formation in engineered systems. In case the precipitation could not be prevented, the knowledge of precipitation reactions and mechanisms could allow to predict the evolution of such systems over large timescales.

Materials and methods

Chemicals

The following chemicals were used: iron (II) sulfate heptahydrate ($FeSO_4 \cdot 7H_2O$, Sigma Aldrich, 99.90 wt.%) as Fe(II) source, fumed silica (SiO_2, Aerosil® 380, Evonik) as silicon source, powder sodium hydroxide (NaOH, Sigma Aldrich, 97 wt.%) to provide an alkaline medium and sodium dithionite ($Na_2S_2O_4$, Alfa-Aesar, 85 wt.%,) to maintain reducing conditions. Deionized water (DIW, 18.2 MΩ·cm) was used for all the experiments.

Synthesis protocol

The protocol is based on a hydrothermal synthesis starting from a suspension having an Fe:Si molar ratio equal to 1.5. Such molar ratio would correspond to a theoretical structure $Si_2Fe_3O_5(OH)_4$ of greenalite and also analogous to natural Mg-rich 1:1 type phyllosilicates. The procedure consisted of dissolving successively in 70 mL of deionized water 0.041 g of $Na_2S_2O_4$,

https://doi.org/10.1180/clm.2024.8 Published online by Cambridge University Press

4.510 g of $FeSO_4 \cdot 7H_2O$ ($[Fe^{2+}] = 0.232$ mol·L^{-1}), 0.647 g of SiO_2 ($[Si] = 0.154$ mol·L^{-1}) and a given quantity of NaOH ($[OH^-] = 0.45$-0.55 mol·L^{-1}) to obtain a given pH (Table S1). Sodium dithionite was added to maintain reduced condition, as mentioned in previous synthesis protocols of similar materials (Harder, 1978; Mizutani *et al.*, 1991). The given amount of NaOH was added for varying the pH. The range of this amount was determined based on our previous study (Boumaiza *et al.*, 2020), where the formation of 1:1 type phyllosilicate was observed with an OH:Fe molar ratio equal to 2.4 . Note that for some experiments the OH:Fe molar ratio was the same, but the measured pH values were slightly different. In practice, it was the obtained pH value that determined the synthesis outcome as demonstrated further by the results. The mixture was stirred during 2 h at room temperature before being sealed in a Teflon-lined stainless-steel mineralization bomb (Top Industrie ®, 150 mL) for two days at 160°C. The synthesis time and temperature were chosen based on our previous study (Boumaiza *et al.*, 2020). After the hydrothermal treatment, the bomb was cooled down until the room temperature. The product was recovered and washed three times with deionized water by dispersion-centrifugation at 8000 rpm for 5 min (9946·*g*) and dried at 60°C. The resulting product mass after washing was about 1.8 g.

The pH of the aged suspensions after 2 hours (pH_i) and of the solutions after the hydrothermal treatment (pH_f) were measured at 25°C using an Orion TM ThermoFisher electrode (pH +/- 0.01) calibrated with two buffer solutions at pH 7.0 and 10.0.

Characterization methods

Powder X-ray diffraction. Data were collected with a powder Bruker diffractometer D8 ADVANCE (Germany) in Bragg-Brentano reflexion geometry θ – θ (goniometer radius is 280 mm). This diffractometer was equipped with the LynxEye XE-T high resolution energy dispersive 1-D detector ($CuK\alpha_{1,2}$). This kind of detector allows to avoid Fe fluorescence effects with Cu X-ray tube. The X-ray diffractograms were recorded in the following conditions: angular area 3-70 °2θ, step size 0.017 °2θ, time per step 1.8 s (total time per step was 345 s), variable divergence slits mode (irradiated sample length 15 mm), total time for acquisition 2 h. During the data collection, powder sample was rotating at 5 rpm. Motorized anti-scatter screen was used for effective suppression of instrument background, most importantly air-scatter at low angles 2θ.

Raman spectroscopy. Raman spectra were obtained with a Horiba LABRAM 300 confocal-Raman spectrometer (France) equipped with a Compass 315M-50 laser (50 mW, 632 nm), diffraction gratings of 600 grooves mm^{-1} and CCD matrix detector. Laser focusing and sample

https://doi.org/10.1180/clm.2024.8 Published online by Cambridge University Press

viewing were performed through Olympus BX40 microscope fitted with x50 objective lens. The spot size was ca 15-20 µm, resolution 4 cm^{-1}. Laser power could be reduced by filters to about 1, 0.1 and 0.01 mW.

Transmission electron microscopy. Powder sample was impregnated in epoxy resin (Bond E-set, Konishi Bond, Japan) and sandwiched between two glass slides to ensure the preferred orientation of sample. The sandwiched sample was sliced and polished mechanically. The TEM lamella (10 µm x 5 µm x ~0.15 µm) was prepared by focused ion beam (FIB) lift-out technique in a dual beam FIB-SEM (Thermo Fisher Scientific Scios and Scios2, USA). The specimens prepared by FIB were characterized using a field-emission transmission electron microscope (FE-TEM; JEOL JEM-2100F HR, Japan) operated at 200kV. High resolution TEM (HRTEM) images were recorded using a Gatan Ultrascan 100XP bottom-mounted CCD camera (USA). Some of the HRTEM images were processed using the Wiener-filter (Marks, 1996; Kilaas, 1998) developed by K. Ishizuka (HREM Research Inc., Japan), which was implemented in a Gatan Digital Micrograph software (USA) to remove noise contrast. Energy dispersive X-ray spectroscopy (EDS) spectrum imaging was performed by a JEOL JED-2300T silicon drift detector equipped on the TEM in scanning TEM (STEM) mode.

Mössbauer spectroscopy. Mössbauer spectrometer was equipped with 512 multichannel analyzer (Halder Electronic Gmbh, Germany) and a 50 mCi source of ^{57}Co in Rh matrix. Mössbauer analysis were performed at 290 K and 12 K with a constant acceleration. Data were obtained from appropriate amounts (10 mg of Fe per cm^2) of solid samples to get optimal experimental conditions. In order to avoid the condensation of oxygen and water on the walls of the cryostat, samples were quickly transferred under inert He atmosphere to a cold-head cryostat, equipped with vibration isolation stand and developed in the LCPME Laboratory. The recordings at 290 K were performed on the spectrometer equipped with the Advanced Research Systems cryostat, while the recordings at 12 K were done on the spectrometer coupled to the Janis Cryostat. Mössbauer spectra were collected in transmission mode. The 50 mCi source of ^{57}Co in Rh matrix was maintained at room temperature (RT) and mounted at end of a Mössbauer velocity transducer. The spectrometer was calibrated with a 25 µm foil of α-Fe at room temperature. Analysis of the Mössbauer spectra consisted of least-square fitting of data with a combination of two-peak quadrupole components (doublets) and, when present, six-peak magnetic hyperfine components (sextets). Most of the time computer fitting with Lorentzian-shape lines is sufficient to fit spectra. However, Voigt profile analysis from Rancourt & Ping

https://doi.org/10.1180/clm.2024.8 Published online by Cambridge University Press

(1991) for quadrupole splitting distribution (QSDs) and magnetic hyperfine fields (HFDs), can be more relevant for analyses of dynamic effects on spectral line broadening.

Calculation of theoretical solubility and speciation of silicon compounds

Table 1 summarizes the equations used to calculate the theoretical solubility and speciation of silicates corresponding to the experimental conditions used during the preparation of the precursor at room temperature.

Table 1. Theoretical concentration C and speciation of amorphous silica in water at 298K.

$C < C_0 = 0.154$ mol/L	**$C = C_0 = 0.154$ mol/L**
$C = [H_4SiO_4] + [H_3SiO_4^-] + [H_2SiO_4^{2-}]$	
$C = \mathbf{10^{-2.7}}\left(\mathbf{1} + \frac{\mathbf{10^{-9.7}}}{\mathbf{10^{-pH}}}\left(\mathbf{1} + \frac{\mathbf{10^{-13.2}}}{\mathbf{10^{-pH}}}\right)\right)$	$C = C_0$
$[H_4SiO_4] = \mathbf{10^{-2.7}}$	$[H_4SiO_4] = \left[\left(\frac{C0}{1+\frac{10^{-9.7}}{10^{-pH}}\left(1+\frac{10^{-13.2}}{10^{-pH}}\right)}\right)\right]$
$[H_3SiO_4^-] = \mathbf{10^{-2.7}}\left[\left(\frac{1+\frac{10^{-9.7}}{10^{-pH}}\left(1+\frac{10^{-13.2}}{10^{-pH}}\right)}{\frac{10^{-pH}}{10^{-9.7}}+1+\frac{10^{-13.2}}{10^{-pH}}}\right)\right]$	$[H_3SiO_4^-] = \left[\left(\frac{C0}{\frac{10^{-pH}}{10^{-9.7}}+1+\frac{10^{-13.2}}{10^{-pH}}}\right)\right]$
$[H_2SiO_4^{2-}] = \mathbf{10^{-2.7}}\left[\left(\frac{1+\frac{10^{-9.7}}{10^{-pH}}\left(1+\frac{10^{-13.2}}{10^{-pH}}\right)}{1+\frac{10^{-pH}}{10^{-13.2}}\left(1+\frac{10^{-pH}}{10^{-9.7}}\right)}\right)\right]$	$[H_2SiO_4^{2-}] = \left[\left(\frac{C0}{1+\frac{10^{-pH}}{10^{-13.2}}\left(1+\frac{10^{-pH}}{10^{-9.7}}\right)}\right)\right]$

where $[H_4SiO_4] = 10^{-2.7}$ mol·kg^{-1} H_2O (solubility constant of amorphous silica is $10^{-2.7}$ at 298 K) (Gunnarsson & Arnórsson, 2000), pKa ($H_3SiO_4^-/H_4SiO_4$) = 9.7 (Alexander *et al.*, 1954) and pKa ($H_2SiO_4^{2-}/H_3SiO_4^-$) = 13.2 (Eikenberg, 1990) and $C_0 = [Si]_{initial} = 0.154$ mol·L^{-1}.

In this study we chose a simple model of silica speciation even if a more realistic speciation of silica species especially at pH>10 has been proposed (Felmy *et al.*, 2001). The suggested model considers dimeric, trimeric (linear, cyclic, and substituted), tetrameric (linear and cyclic), and hexameric (prismatic) species in addition to monomeric ones. However, the monomeric species

https://doi.org/10.1180/clm.2024.8 Published online by Cambridge University Press

remain the major species in solution, and could be considered therefore as a good first approximation.

Measurements of electrolytic conductivity

The conductimetry experiments were conducted with a conductimeter PC 5000 L Phenomenal, VWR, Radnor, US. The ionic conductivity of the solution was assumed to be the sum of the specific conductivity of each ion in solution. Each chemical contribution was investigated by measuring the conductimetry of the solution in function of the amount of added OH^-. Two experiments were performed: (1) addition of a given amount of 1M NaOH solution in deionized water; (2) addition of a given amount of 1M NaOH solution in deionized water containing 0.647 g of fumed silica (SiO_2, Aerosil® 380, Evonik).

Results

Mineralogical composition of synthesis products: identification of 3 domains

The XRD powder analysis of the products revealed three distinct domains that differed by the nature of phyllosilicates obtained (Fig.1). For lower OH:Fe ratio (below 2.10) corresponding to $pH_i < 9.67$, XRD showed the presence of some broad yet characteristic peaks of *hkℓ* reflections of phyllosilicates, but the peaks of *00ℓ* reflections were not observable. For higher OH:Fe molar ratio (between 2.10 and 2.16) corresponding to pH_i between 9.67 and 10.75, the 1:1 type phyllosilicate could be identified by its characteristic peak at 7 Å. At high OH:Fe ratio (above 2.16) leading to pH_i that exceeded 10.75, both 1:1 and 2:1 type phyllosilicates were identified in the synthesis products characterized by the peaks at 7 Å and 12 Å, respectively. It has to be noted that all the synthetized products contained iron oxide and/or hydroxide phases. Some of the samples contained thenardite (Na_2SO_4), which formed from the sulfate anions and sodium cations, and had remained due to incomplete washing. A more detailed characterization of three samples representing each domain, was further carried out by powder XRD, Raman and Mössbauer spectroscopies and transmission electron microscopy.

https://doi.org/10.1180/clm.2024.8 Published online by Cambridge University Press

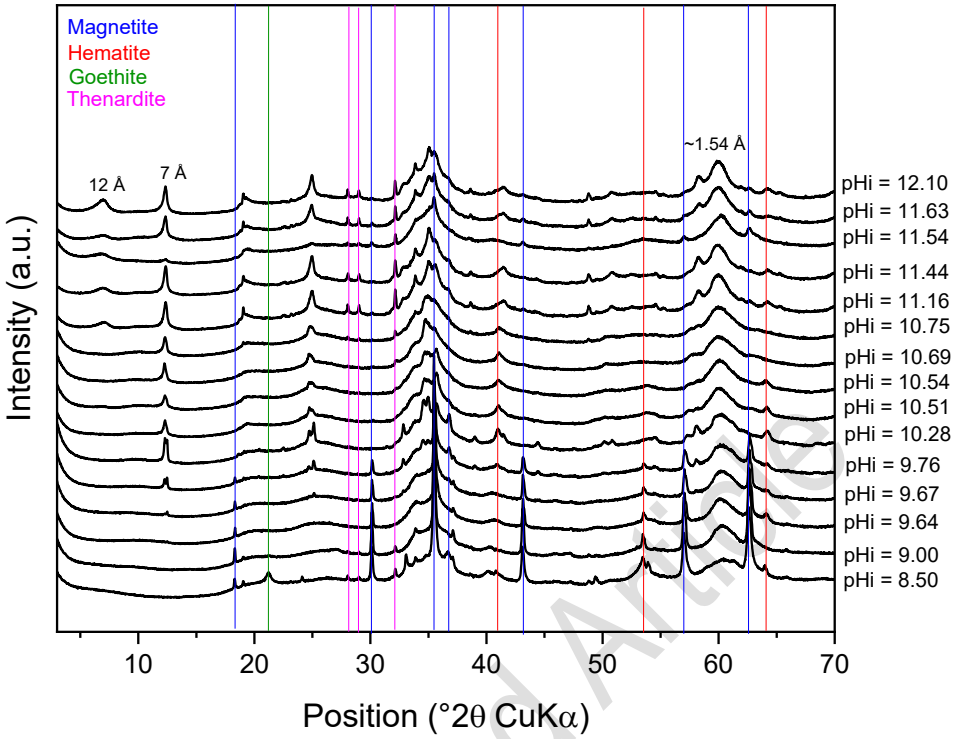

Figure 1 . Powder X-ray diffractograms of synthesis products obtained by varying OH:Fe initial molar ratio from 1.93 to 2.39 (pH_i between 8.50 and 12.10).

Characterization of synthesis products in domain "1" where $pH_i < 9.67$

A sample prepared with a pH_i value of 8.50, representing domain 1, was chosen for a more detailed characterization. The powder X-ray diffractogram revealed reflections at 4.84 Å (18.28 °2θ), 2.78 Å (32.17 °2θ) and 2.09 Å (43.14 °2θ) corresponding to magnetite (Fig.2A). The characteristic reflections of hematite at 2.69 Å (33.15 °2θ) and at 1.45 Å (64.02 °2θ) and of goethite at 4.17 Å (21.28 °2θ) were also identified. Broad peaks corresponding to the diffraction angles of phyllosilicates' planes at 2.57 Å (34.32 °2θ) and at 1.52 Å (60.37 °2θ) suggested the formation of poorly crystalline phyllosilicate phase (Stucki *et al.*, 1989). The high signal intensity above the baseline, suggested the presence of amorphous compounds in the sample, such as amorphous silica.

https://doi.org/10.1180/clm.2024.8 Published online by Cambridge University Press

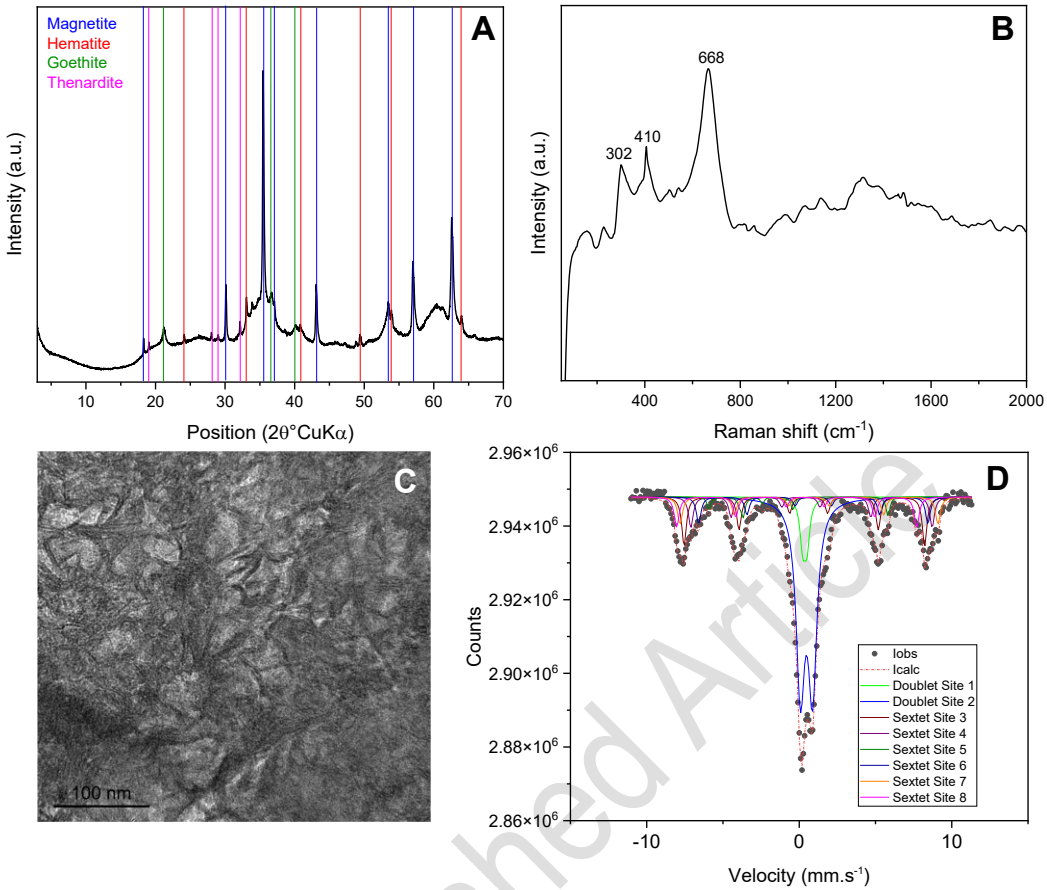

Figure 2. X-ray diffractogram (A), Raman spectrum (B), TEM image (C) and Mössbauer spectrum at 12 K (D) of sample with pH_i = 8.50.

Raman spectroscopy confirmed the presence of magnetite with characteristic bands at 302 cm^{-1} and 668 cm^{-1} (de Faria *et al.*, 1997) (Fig.2B). The hematite and goethite phases could not be detected probably due to their low amount in the sample.

Well-crystalline clay structure was not observed in TEM. Only low-crystalline phase with sheet-like texture was seen (Fig. 2C). Selected area electron diffraction (SAED) pattern gave a halo ring pattern characteristic for a low crystalline phase (Fig.S1 in Supplementary information). No significant change in the SAED pattern and high resolution TEM image was observed during the continuous illumination of electron beam. Moreover, Ga contamination by the FIB was negligible in the analyzed area. These results indicate that the low-crystalline phase was not formed by the beam damage during the specimen preparation process by FIB nor TEM observation. The chemical analysis of this area yielded molar Fe:Si=0.73 suggesting that this low-crystalline phase could correspond then to 2:1 type phyllosilicate-like structure. This observation agrees with results of X-ray diffraction (Fig. 2A), where no peak of 001 reflection,

https://doi.org/10.1180/clm.2024.8 Published online by Cambridge University Press

characteristic for phyllosilicates, was observed, and only broad reflections around 35 and 60 °2θ (corresponding to 2.6 and 1.53 Å, respectively) were recorded. The absence of 00ℓ reflections in X-ray diffractogram indicates that the stacking of layers is absent. Indeed, the TEM observation revealed a phase with sheet-like texture, but small size and only few layers thick.

The deconvolution of Mössbauer spectrum acquired at room temperature confirmed the presence of various iron bearing phases: magnetite, goethite and iron-rich phyllosilicate (Fig. S2 and Table S2 in Supplementary information). These results were in agreement with mineralogical composition identified by powder X-ray diffraction. The phyllosilicate phase contained two Fe(III) components, which could be attributed to both the octahedral and tetrahedral sites (Dyar *et al.*, 2006). The spectrum recorded at low temperature (Fig. 2D) confirmed the nature of observed phases at room temperature (Fig.S2 in Supplementary Information). The iron oxide components' contribution to the recorded signal was more important, as expected, for low temperature (Table 2). The sextet characterized by magnetic field of 487 kOe and negative quadrupole shift ε (- 0.28 mm/s) was attributed to goethite (Murad & Johnston, 1987; Benali *et al.*, 2001), while the five other sextets can be assigned to magnetite as established for this mineral at very low temperature in the literature (Vandenberghe *et al.*, 2000; Meite *et al.*, 2022).

Table 2. Mössbauer parameters for the synthesis product with $pH_i = 8.50$ at 12 K, where CS is center shift, Δ is quadrupole splitting, H is hyperfine field, and R.A. is relative abundance.

	CS (mm/s)	Δ or Ɛ (mm/s)	H (kOe)	R.A. (%)	
Doublet (1)	0.36	0.27		6	Fe(III) in phyllosilicate
Doublet (2)	0.48	0.76		45	Fe(III) octahedral in phyllosilicate
Sextets	0.48	-0.139	488	12	Magnetite
	0.44	0.36	490	8	
	1.04	2.11	294	5	
	0.93	0.05	465	8	
	0.62	0.03	523	8	
Sextet	0.32	-0.28	487	8	Goethite

Considering the obtained chemical analysis from EDS (Table 3) and iron oxidation state obtained from Mössbauer spectroscopy at 12 K, the formula of the phyllosilicate in domain 1 could be estimated as $Fe^{III}_{2.16}(Si_{3.51}Fe^{III}_{0.49})O_{10}(OH)_2$ corresponding to 2:1 type phyllosilicate-like phase. It has to be noted that more detailed tests such as cation exchange experiments would allow to establish a more realistic formula. However, for such experiments a pure phase would be needed, which is not the case here. Nevertheless, the characterizations done in this study

https://doi.org/10.1180/clm.2024.8 Published online by Cambridge University Press

allow to suggest a first approximate estimation of the obtained phase. In summary, the samples obtained in this domain contained magnetite, goethite and poorly crystalline 2:1 type Fe(III)-rich phyllosilicate-like phase.

Table 3. Chemical composition of samples.

pHi	8.50	10.28	11.63	
Type of structure	2:1	1:1	1:1	2:1
SiO_2	52.49	27.29	38.06	38.53
FeO*	47.51	72.71	61.94	61.47
Total	100.00	100.00	100.00	100.00
$Fe^{3+}/\Sigma Fe$ by MS	1.00	0.87	0.88	0.88
O =	11	7	7	11
Si	3.51	1.35	1.77	2.80
Fe^{3+} (IV)**	0.49	0.65	0.23	1.20
Σ Tetrahedral cations	4.00	2.00	2.00	4.00
Fe^{2+}	-	0.39	0.29	0.45
Fe^{3+} (VI)	2.16	1.96	1.88	2.10
Σ Octahedral cations	2.16	2.35	2.17	2.55
Number of octahedral vacancies	0.84	0.65	0.83	0.45

* Total iron as FeO. ** Tetrahedral Fe^{3+} was determined assuming there is no tetrahedral vacancy.

Characterization of synthesis products in domain "2" with $9.67 \leq pH_i \leq 10.75$

For domain "2", sample with pH_i=10.28 was chosen for more detailed characterization. XRD traces revealed the presence of the phyllosilicate of 1:1 type with its main peak at 7 Å (12.44 °2θ) and other peaks at 3.56 Å (25.01 °2θ) and 1.53 Å (60.40 °2θ) (Fig.3A). A broad peak around 10 °2θ suggested possibly a second poorly ordered 1:1 type phyllosilicate phase. Peaks of hematite were also detected at 1.45 Å (64.22 °2θ) and 1.69 Å (54.49 °2θ) respectively. Raman data confirmed the presence of hematite with characteristic intensive bands at 223, 293, 410, 507, 610 and 1321 cm^{-1} (de Faria *et al.*, 1997) (Fig.3B). Observation in TEM revealed the layered structure characteristic of 1:1 phyllosilicate with an average basal spacing of 7 Å (Fig.3C). SAED pattern confirmed a periodicity of 7 Å (Fig. S3 in Supplementary information). The chemical analysis of the area yielded molar Fe:Si ratio of 1.71 (the initial ratio was 1.50).

https://doi.org/10.1180/clm.2024.8 Published online by Cambridge University Press

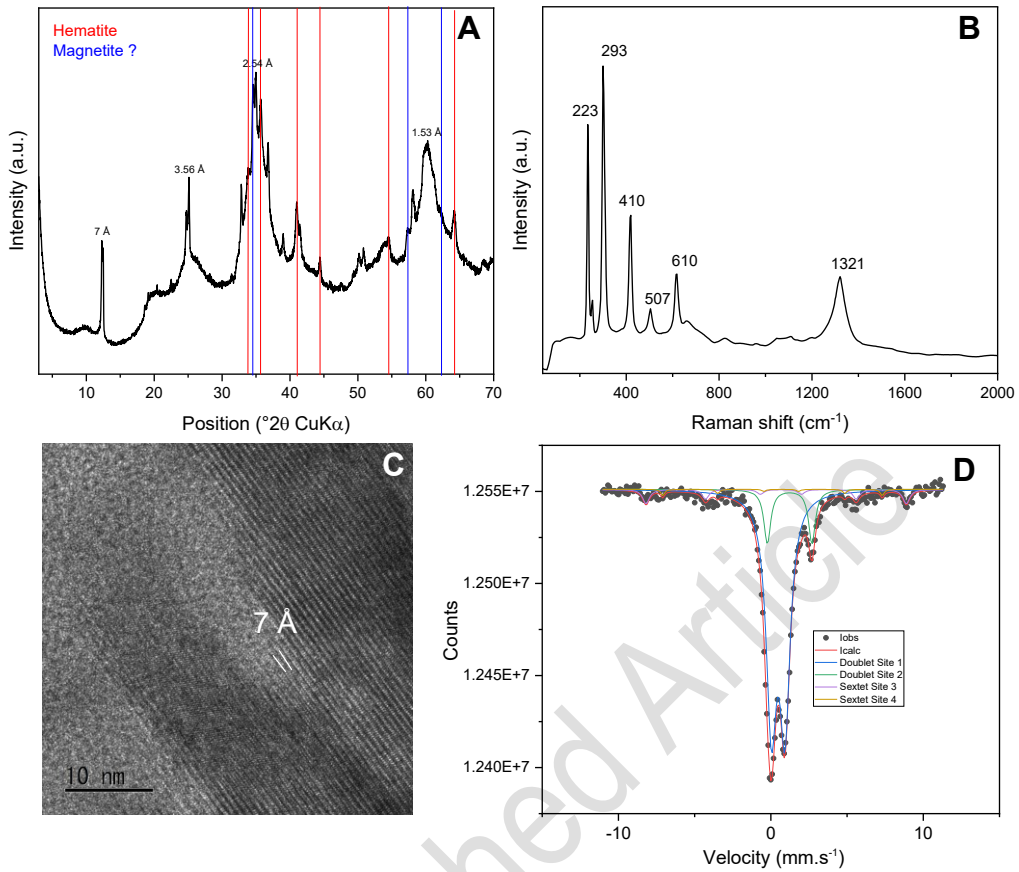

Figure 3. X-ray diffractogram (A), Raman spectrum (B), TEM image (C) and Mössbauer spectrum at 13 K (D) of sample with pH_i = 10.28.

The Mössbauer spectrum at room temperature revealed two components corresponding to Fe(III) and Fe(II) in phyllosilicate structure (Fig. S4 and Table S3 in Supplementary Information). The spectrum at low temperature revealed also the presence of iron oxide phase (hematite) (Fig.3D and Table 4).

Table 4. Mössbauer parameters for the synthesis product with pH_i = 10.28 at 13 K, where CS is center shift, Δ is quadrupole splitting, and R.A. is relative abundance.

	CS (mm/s)	Δ or Ɛ (mm/s)	H (kOe)	R.A. (%)	
Doublet (1)	0.48	0.88		79	Fe(III) in phyllosilicate
Doublet (2)	1.23	2.92		12	Fe(II) in phyllosilicate
Sextet (3)	0.50	-0.15	529	7	Iron oxide (hematite)
Sextet (4)	0.39	-0.05	450	2	Iron oxide (hematite)

Considering the obtained chemical analysis from EDS (Table 3) and iron oxidation state obtained from Mössbauer spectroscopy at 13 K, the formula of phyllosilicate in domain 2 could

https://doi.org/10.1180/clm.2024.8 Published online by Cambridge University Press

be estimated as $Fe^{II}_{0.39}Fe^{III}_{1.96}(Si_{1.35}Fe^{III}_{0.65})O_5(OH)_4$ corresponding to serpentine-like structure. Although the tetrahedrally coordinated Fe^{3+} was not suggested by the Mössbauer spectroscopy, it is reasonable to assume that there is no vacant site in tetrahedral sites. Therefore, some of the Fe^{3+} was assigned in the tetrahedral site. In summary, samples obtained in this domain were composed of hematite and serpentine-like phyllosilicate.

Characterization of synthesis products in domain "3" with $pH_i > 10.75$

The sample with $pH_i = 11.63$ was studied in detail. XRD data showed the presence of two types of phyllosilicates: 2:1 type and 1:1 type, identified by their characteristic peaks at 12 Å and 7 Å, respectively. Some broad reflections corresponding to iron oxides, magnetite and/or hematite, were identified. The diffraction peaks at 4.65 Å (19.05°2θ) 3.17 Å (28.14°2θ) and 3.07 Å (29.04°2θ) corresponded to thenardite (Na_2SO_4) attributed to the use of sodium hydroxide and the ferrous sulfate as precursors (Fig.4A). Raman spectrum corresponded to the one of hematite with the characteristic peaks as reported for the domain "2" (Fig.4B).

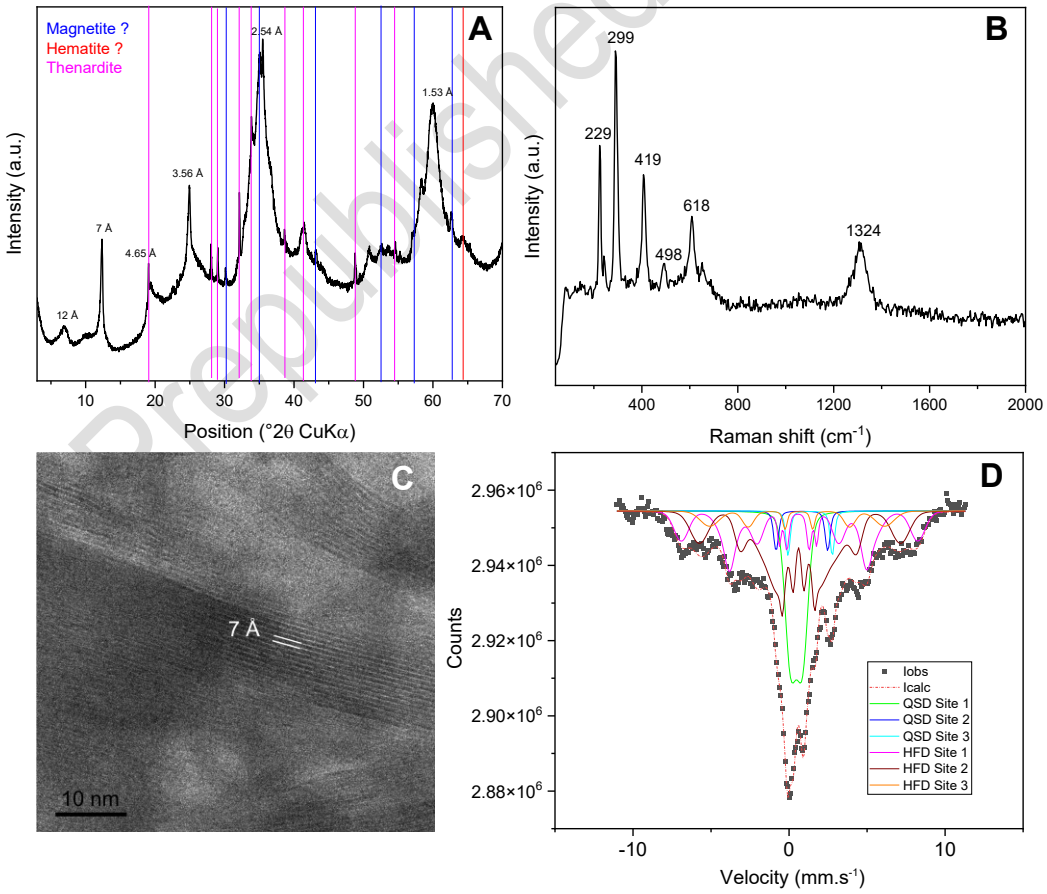

https://doi.org/10.1180/clm.2024.8 Published online by Cambridge University Press

Figure 4. X-ray diffractogram (A), Raman spectrum (B), TEM image (C) and Mössbauer spectrum at 11 K (D) of sample with pH_i = 11.63.

The observation of particles in TEM revealed a clay mineral-like phase with 7 Å periodicity (Fig.4C). Also, low crystallinity regions were observed (Fig.S5 in Supplementary information) with sheet-like texture. Indeed, the 2:1 phyllosilicate phase identified by XRD had broad peaks suggesting poor crystallinity in agreement with observations under TEM (Fig. S5 in Supplementary information).

The deconvolution of Mössbauer spectrum obtained at room temperature could be deconvoluted in 4 components corresponding to two types of sites of Fe(III) and two types of sites of Fe(II) (Fig. S6 and Table S4 in Supplementary information). Considering the presence of 2:1 and 1:1 types phyllosilicates in the sample, at least part of the Fe(III) and Fe(II) sites observed on the RT spectrum belong to the phyllosilicate phase. The Mössbauer spectrum at low temperature differed significantly from the one at room temperature. Additional magnetic components composed of three sextets (and absent at ambient) appeared at the low temperature spectrum (Fig.4D). As a consequence, the relative abundance of paramagnetic components of Fe(III) decreased from 80% in room temperature spectrum to only 21% at low temperature (Table 5). Such behavior confirmed the presence of poorly crystalline iron oxides in the sample as suspected from the broad peaks in X-ray diffractogram and evidenced by Raman spectroscopy or on the basis of relaxation phenomena observed in magnetic structures obtained at low temperatures and due to the superparamagnetic behavior of iron oxides as obtained by Meite *et al.* (2022). However, the phenomenon of superparamagnetism, which is a good indication of the small size of the particles, as also suggested by XRD and TEM, may render interpretation more difficult.

Table 5. Mössbauer parameters for the synthesis product with pH_i = 11.63 at 11 K, where CS is center shift, Δ is quadrupole splitting, and R.A. is relative abundance.

	CS (mm/s)	Δ or Ɛ (mm/s)	H (kOe)	R.A. (%)	
Doublet (1)	0.47	0.83		21	Fe(III) in phyllosilicate
Doublet (2)	0.82	3.3		3	Fe(II) in phyllosilicate
Doublet (3)	1.35	2.84		3	Fe(II) in phyllosilicate
Sextet (4)	0.62	0.05	360	25	Iron oxide
Sextet (5)	0.65	0.04	224	41	Iron oxide
Sextet (6)	0.57	-0.05	380	7	Iron oxide

https://doi.org/10.1180/clm.2024.8 Published online by Cambridge University Press

The chemical composition of phyllosilicate-like phases was estimated by TEM-EDS analyses of 7 Å and poorly crystalline regions of particles (Table 3). In both cases, molar Fe:Si ratio was between 1.32 and 1.36. Assuming that doublet (3) (Table 5) would correspond to 1:1 phyllosilicate phase and doublet (2) would correspond to 2:1 phyllosilicate-like phase, an estimation of formula was attempted. For 1:1 phyllosilicate-like phase it gave $Fe^{II}_{0.29}Fe^{III}_{1.88}(Si_{1.77}Fe^{III}_{0.23})\,O_5(OH)_4$ corresponding to serpentine-like phase similar to the one obtained for the domain 2, and for the 2:1 phyllosilicate-like phase it gave $Fe^{II}_{0.45}Fe^{III}_{2.10}(Si_{2.80}Fe^{III}_{1.20})O_{10}(OH)_2$ corresponding to 2:1 type phyllosilicate-like phase. In summary, the samples obtained in this domain contained phyllosilicate-like phases of serpentine and 2:1 phyllosilicate type, and possibly hematite, which was detected by Raman and Mössbauer spectroscopies.

Evolution of pH: correlation with 3 domains of distinct mineralogical composition

The pH of medium was measured after 2 hours of the aging of precursor (pH_i) and after the hydrothermal treatment (pH_f). It has to be noted that the pH after the addition of reactants (pH_0) in all samples was higher than pH_i. Three domains were identified which differed between them with respect to the evolution between pH_i and pH_f (Fig. 5). The identified domains here correlated to the ones identified with respect to the mineralogical composition in Fig.1.

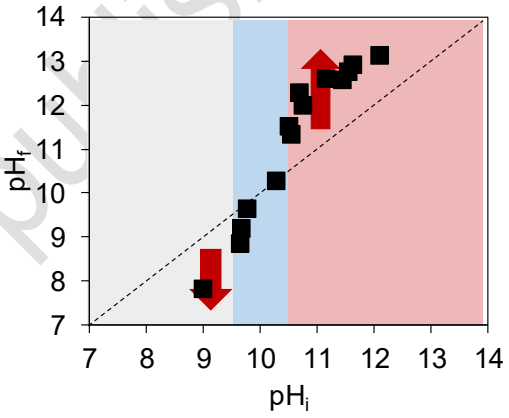

Figure 5. Comparison between pH after hydrothermal treatment (pH_f) with pH after aging of precursor (pH_i).

In the first domain where $pH_i \leq 9.67$, the final pH was lower compared to the pH_i. It suggested the consumption of OH^- and/or the production of H^+. These ions were used in the condensation reactions resulting in the formation of iron oxides minerals: magnetite, hematite and goethite (Schwertmann & Cornell, 2000). These phases were identified by different characterization techniques (Fig. 2). In the second domain, where $9.60 < pH_i < 10.75$, the pH remained stable throughout the experiment, and did not change after the hydrothermal treatment. During the

https://doi.org/10.1180/clm.2024.8 Published online by Cambridge University Press

precipitation reactions, the amount of consumed OH^- was then expected to be equal to the amount of the released OH^-. This domain corresponded to the precipitation of 1:1 type phyllosilicate (Fig.3). In the third domain, where $pH_i \geq 10.75$, the pH after the hydrothermal treatment increased with respect to the pH after the aging of the precursor. It suggested the release of OH^-, as a result of reactions leading to the precipitation of both 1:1 and 2:1 type phyllosilicates (Fig.4). It has to be noted that the overall amount of OH^- in solution decreased with respect to the initially introduced amount. However, during the aging of the precursor more OH^- was consumed with respect to what is needed to phyllosilicate precipitation only. It can be explained by the consumption of OH^- to solubilize silica and to associate with iron(II) aqueous species. This amount of OH^- initially consumed was then partially released when the formation of phyllosilicates occurred.

Theoretical solubility of silica compounds and speciation of dissolved silica species in function of pH

According to the literature (Gunnarsson & Arnórsson, 2000), the solubility constant of amorphous silica is $10^{-2.7}$ at 298 K. The theoretical solubility for dissolved silica was calculated from the equation in Table 1, which is represented in Fig.6A. It can be seen then, when pH < 9.0 the amount of dissolved silica is very low, and when pH > 11.6 all the initial amount of silica is dissolved.

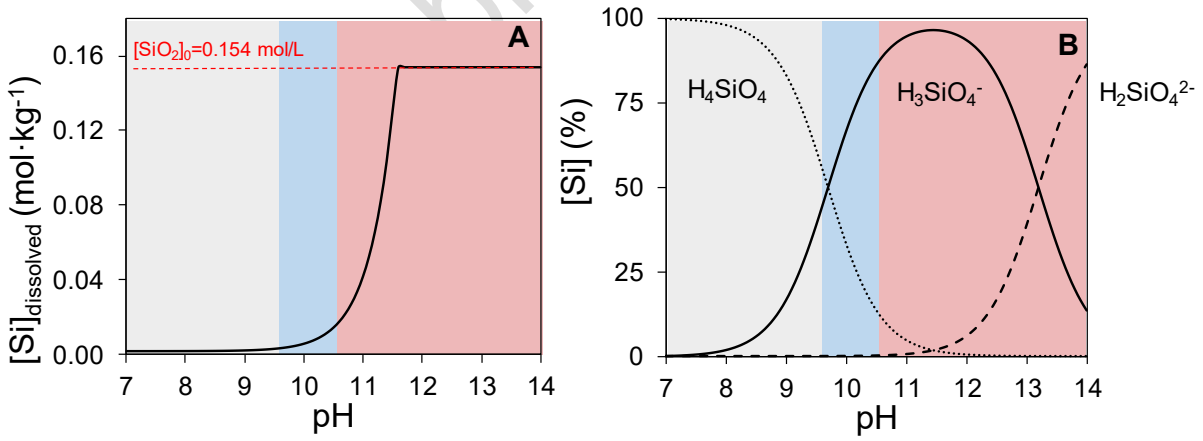

Figure 6. Theoretical solubility of amorphous silica (A) and speciation of silica aqueous species (B) as a function of pH at 298 K.

In domain 1, the formation of iron oxyhydroxides was observed. The very low solubility of silica could explain the absence of well crystallized phyllosilicates, and the presence of residual amorphous silica. Indeed, an amorphous silica could be a precursor of iron-rich phyllosilicates (Francisco *et al.*, 2020). The increase of solubility of silica correlated with the presence of

https://doi.org/10.1180/clm.2024.8 Published online by Cambridge University Press

crystalline phyllosilicate phases in synthesized samples observed in domains 2 and 3. The availability of dissolved silica species favoured the reactions leading to the precipitation of phyllosilicates.

Interestingly, that the precipitation of 1:1 phyllosilicate-type was observed only above pH 9.7. It could be related to the net increase of the solubility of amorphous silica above this value. However, in domain 1 the precipitation of phyllosilicate of 2:1 type was identified. The formation of 2:1 phyllosilicate requires more silicon compared to the formation of 1:1 type phyllosilicate. It has to be noted, that the precipitated 2:1 type phyllosilicate was poorly crystalline due to the small quantity of silica available. However, despite the low quantity of silica aqueous species available, 2:1 type phyllosilicate still formed, suggesting that the solubility of amorphous silica would determine only the crystallinity of phyllosilicate formed, but not their type.

The lower limit for the formation of 1:1 phyllosilicate-type correlates with silica aqueous speciation (Fig.6B). From pH 9.7 to 13.2 the main species in solution is trihydrogen orthosilicate ($H_3SiO_4^-$). Below pH 9.7 the predominant species is silicic acid (H_4SiO_4). Above pH 13.2 the dissolved silica is mainly in the form of dihydrogenorthosilicate ($H_2SiO_4^{2-}$). The coincidence of the formation of 1:1 type phyllosilicate with lower limit of predominance of trihydrogen orthosilicate ($H_3SiO_4^-$) at pH = 9.7 suggests then the presence of this specie in solution is necessary for the formation of 1:1 phyllosilicate type particles.

Experimental solubility of silica in function of $[OH]^-_{introduced}$ determined by the measure of electrolytic conductivity

Conductivity is proportional to the amount of charged species in solution. Indeed, when a given amount of OH^- ions is introduced with 1M NaOH solution, a linear relationship is found (black filled dots in Fig. 7A). When the same experiment is repeated in the presence of amorphous silica (empty rectangles in Fig. 7A), a linear trend is also observed, but the conductivity of solution decreased this time due to the consumption of OH^- used to dissolve SiO_2.

https://doi.org/10.1180/clm.2024.8 Published online by Cambridge University Press

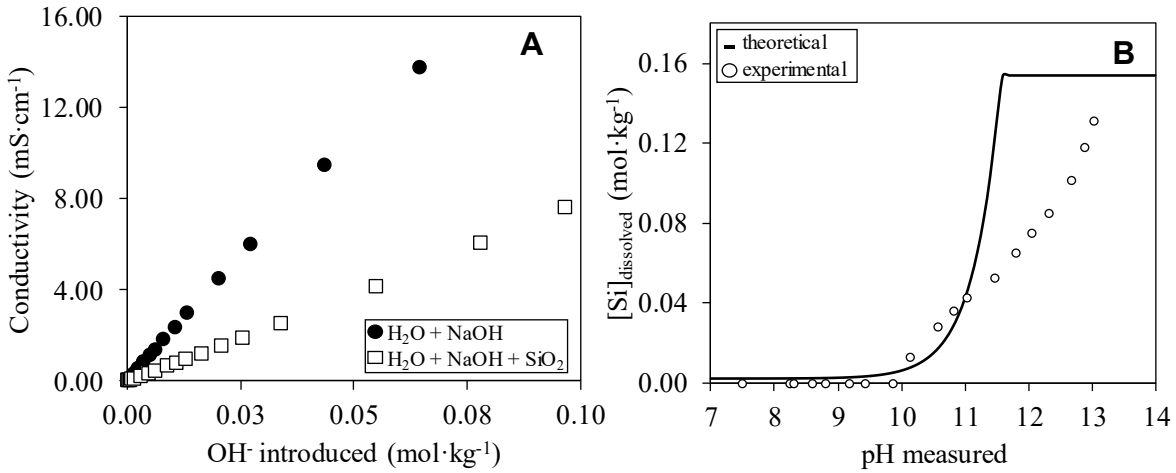

Figure 7. Solution conductivity as a function of the amount of OH^- introduced (A), and a comparison between theoretical and calculated solubility of silica (B) as a function of pH at 298 K.

Knowing the amount of OH^- consumed to dissolve SiO_2, the amount of $[Si]_{dissolved}$ can then be calculated (empty circles, Fig. 7B). The dissolved amount of Si thus obtained can be then compared to the theoretical solubility of silica as a function of pH (black line, Fig. 7B). The calculated amount of dissolved SiO_2 from conductivity measurement, follows the same trend as the theoretical solubility of silica. The experimental amount of dissolved Si is probably overestimated between 10 and 11 due to important uncertainties related to the pH measurements. Above pH 11, the calculated amount of dissolved SiO_2 from conductivity measurement increases similarly as the theoretically predicted amount. The difference between the experimentally dissolved silica and theoretically predicted should be due to the dissolution kinetics of SiO_2 (Gong *et al.*, 2022). Indeed, the conductivity measurements were done instantly after the addition of NaOH. The silica dissolution experiment revealed that in addition to silica solubility and speciation, the kinetics of silica solubility should be taken in consideration as well. However, this may help to understand which type of phyllosilicate is formed depending on the amount of dissolved silica. In Domain II, due to the small amount of silica dissolved, 1:1 phyllosilicate phases are formed, whereas in Domain III, 2:1 phyllosilicate phases, which need more silicon, are formed due to a higher amount of silica dissolved. It has to be noted, that poorly crystalline 2:1 phyllosilicate-like phase formed also in Domain I despite a very small amount of silica dissolved.

Discussion

Fig. 8 summarizes the mineral phases detected in each domain of pH in the synthesis products.

https://doi.org/10.1180/clm.2024.8 Published online by Cambridge University Press

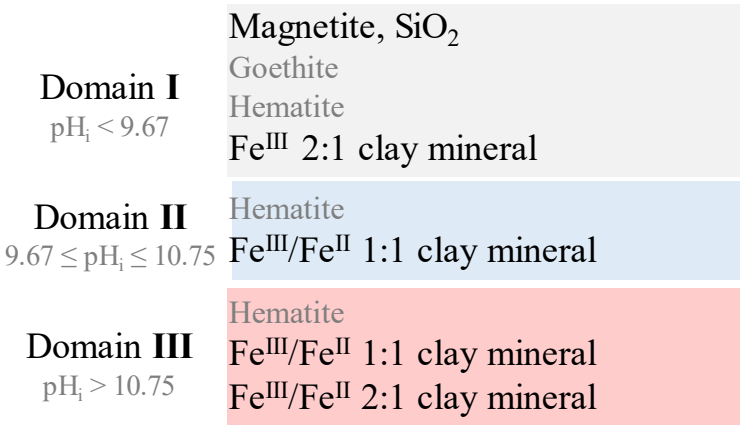

Figure 8. Summary of characteristic mineral phases identified in each pH domain.

Although working in air, the results showed that part of Fe ions introduced in the reaction mixture as iron (II) sulfate, stayed as Fe(II) throughout the experiment, and was incorporated as such in neo-formed mineral phases. The presence of hematite in all samples, suggested partial oxidation of Fe(II) to Fe(III). Different reaction pathways can lead to the formation of hematite (Schwertmann & Cornell, 2000). It could have formed from goethite during the hydrothermal treatment, or precipitated in hydrolysis and condensation reactions from Fe(III) containing solution during the aging of the precursor (*cf,* Supplementary Information reaction 2 and 3) or by oxidation of magnetite. The presence of hematite thus indicates that some of the Fe(II) initially introduced in the reaction mixture underwent oxidation, but it could have happened at different moments.

The formation of phyllosilicate-like compounds occurred throughout all range of pH, but the crystallinity and type could be correlated to the solubility and speciation of silica, which in turn is governed by the solution pH. At acidic pH and weakly basic solution below pH 9, the solubility of silica is very low and the main species in solution is H_4SiO_4, and poorly crystalline Fe^{III}-bearing 2:1 phyllosilicate was identified. A possible precipitation equation is given in Supplementary information, reaction 4. This finding is in agreement with previous studies regarding glass corrosion, where a 2:1 type phyllosilicate phase (nontronite-like) and/or iron oxides were identified (Carriere *et al.*, 2021; Kikuchi *et al.*, 2022; Galai *et al.*, 2023). It is important to note that the 2:1 type phyllosilicate like phase was poorly crystallized and can be considered amorphous (Fig S1. in Supplementary information). It could be easily overlooked if the sample is studied by usual characterization techniques such as an X-ray diffractometer with a copper lamp. In our case we used a high resolution energy dispersive 1-D detector equipment for XRD to reduce iron fluorescence contribution from the sample. However, the presence of

https://doi.org/10.1180/clm.2024.8 Published online by Cambridge University Press

this phase can be an important indicator of an ongoing glass corrosion or be present in silica rich solution conducting pipes.

Above pH 9, the solubility of silica increases and well crystalline phyllosilicate-like phases were obtained. The type of the phase could be correlated to the amount of dissolved silica available and its speciation. The formation of 1:1 phyllosilicate-like phase coincided with the presence of $H_3SiO_4^-$ species in solution above pH 9.5, and low amount of H_4SiO_4. A possible precipitation equation is given in Supplementary Information, reaction (5). Previous studies (Pignatelli *et al.*, 2014; Tosca *et al.*, 2016; Hinz *et al.*, 2021) have also reported the formation of serpentine-like phases around this pH, albeit closer to neutral pH, i.e. 7-8.

In basic pH above 11, silica is found in soluble species form mainly as $H_3SiO_4^-$ and in a low amount as $H_2SiO_4^{2-}$. It has to be noted that in our experiment, some of Aerosil might not had dissolved completely due to kinetics. Indeed, conductimetry measurements showed that more than 6 hours would be needed to solubilize entirely the initially introduced amount of silica. However, when more important amount of silicon is present in solution in soluble form, both types of phyllosilicates were observed to form, Fe^{III}/Fe^{II} bearing 1:1 phyllosilicate and Fe^{III}/Fe^{II} bearing 2:1 phyllosilicate. Possible precipitation equations are given in supplementary information, reactions (6) and (7). Mössbauer spectroscopy results could differentiate between Fe(II) and Fe(III) components, and two Fe(II) components were identified. However, the question remains which component would belong to 1:1 and which to 2:1 type phase. Although the distinction between iron oxides (magnetically ordered) and phyllosilicates (paramagnetic) is straightforward at low temperature, the fact remains that mixtures of phyllosilicates are prone to complicate or affect their respective identification on the basis of their paramagnetic components alone and their oxidation state or Fe atomic environment information (center shift,CS, and quadrupole splitting, Δ). Consequently, structural characterization tools (XRD, TEM) remain essential if samples are not affected by crystallinity problems. The best situation is to complement the results from Mössbauer spectroscopy with these mineralogical structural methods.

In precipitation reactions given in supplementary information, we had assumed that iron was in a form of Fe^{2+} in solution (we used $FeSO_4 \cdot 7H_2O$ as an iron source), but very likely some of iron was actually in a form of Fe^{3+}. Indeed, the study of Hinz *et al.* (2021) mention that the presence of Fe^{3+} is necessary to trigger the precipitation of greenalite (1:1 phyllosilicate belonging to serpentine group). The repartition between Fe^{2+} and Fe^{3+} in precursor solution would govern the necessity to add O_2 to the reactants or H_2 to the products to establish truly representative precipitation reactions. In perspective, an exact knowledge of the amount of Fe^{2+}

https://doi.org/10.1180/clm.2024.8 Published online by Cambridge University Press

and Fe^{3+} in the precursor solution, would allow to establish precipitation equations and give information about the possible formation conditions of such phases.

Conclusion

The influence of pH for the hydrothermal synthesis of iron-rich phyllosilicates was investigated in this study. The findings showed that pH governed crystallinity and nature of obtained phyllosilicate-like phases. Three domains of pH were identified, and correlated with the silica availability and speciation in the solution: domain I with $pH_i<9.67$, domain II with $9.67<pH_i<10.75$ and domain III with $pH_i>10.75$. The formation of 1:1 iron-rich phyllosilicate coincided with the low presence of $H_3SiO_4^-$ aqueous species above pH 9.5. For higher pH and higher amounts of $H_3SiO_4^-$ aqueous species, both 1:1 and 1:2 iron-rich phyllosilicate were found. In future, the knowledge of the quantity of Si, Fe^{2+} and Fe^{3+} in the solution at every stage of process, would allow a better understanding of phyllosilicate-like phase precipitation mechanisms.

References

Alexander, G.B., Heston, W.M. & Iler, R.K. (1954) The Solubility of Amorphous Silica in Water. *The Journal of Physical Chemistry*, **58**, 453–455.

Baron, F., Petit, S., Tertre, E. & Decarreau, A. (2016) Influence of Aqueous Si and Fe Speciation on Tetrahedral Fe(III) Substitutions in Nontronites: a Clay Synthesis Approach. *Clays and Clay Minerals*, **64**, 230–244.

Benali, O., Abdelmoula, M., Refait, P. & Génin, J.-M.R. (2001) Effect of orthophosphate on the oxidation products of Fe(II)-Fe(III) hydroxycarbonate: the transformation of green rust to ferrihydrite. *Geochimica et Cosmochimica Acta*, **65**, 1715–1726.

Bertoldi, C., Dachs, E., Cemic, L., Theye, T., Wirth, R. & Groger, W. (2005) The Heat Capacity of the Serpentine Subgroup Mineral Berthierine (Fe2.5Al0.5)[Si1.5Al0.5O5](OH)4. *Clays and Clay Minerals*, **53**, 380 – 388.

Boumaiza, H., Dutournié, P., Le Meins, J.-M., Limousy, L., Brendlé, J., Martin, C., Michau, N. & Dzene, L. (2020) Iron-rich clay mineral synthesis using design of experiments approach. *Applied Clay Science*, **199**, 105876.

Carriere, C., Neff, D., Martin, C., Tocino, F., Delanoë, A., Gin, S., Michau, N., Linard, Y. & Dillmann, P. (2021) AVM nuclear glass/steel/claystone system altered by Callovo–Oxfordian poral water with and without cement–bentonite grout at 70°C. *Materials and*

https://doi.org/10.1180/clm.2024.8 Published online by Cambridge University Press

Corrosion, **72**, 474–482.

Criouet, I., Viennet, J.C., Baron, F., Balan, E., Buch, A., Delbes, L., Guillaumet, M., Remusat, L. & Bernard, S. (2023) Influence of pH on the Hydrothermal Synthesis of Al-Substituted Smectites (Saponite, Beidellite, and Nontronite). *Clays and Clay Minerals,* **71**(5), 539–558.

Cundy, C.S. & Cox, P.A. (2005) The hydrothermal synthesis of zeolites: Precursors, intermediates and reaction mechanism. *Microporous and Mesoporous Materials*, **82**, 1–78.

Decarreau, A. & Bonnin, D. (1986) Synthesis and Crystallogenesis at Low Temperature of Fe(III)-Smectites by Evolution of Coprecipitated Gels: Experiments in Partially Reducing Conditions. *Clay Minerals*, **21**, 861–877.

Doelsch, E., Rose, J., Masion, A., Bottero, J.Y., Nahon, D. & Bertsch, P.M. (2002) Hydrolysis of Iron(II) Chloride under Anoxic Conditions and Influence of SiO 4 Ligands. *Langmuir*, **18**, 4292–4299.

Dyar, M.D., Agresti, D.G., Schaefer, M.W., Grant, C.A. & Sklute, E.C. (2006) Mössbauer spectroscopy of Earth and planetary materials. *Annual Review of Earth and Planetary Sciences*, **34**, 83–125.

Dzene, L., Brendlé, J., Limousy, L., Dutournié, P., Martin, C. & Michau, N. (2018) Synthesis of iron-rich tri-octahedral clay minerals: A review. *Applied Clay Science*, **166**, 276–287..

Eikenberg, J. (1990) *On the problem of silica solubility at high pH*. Würenlingcn und Villigen, 59 pp.

de Faria, D.L.A., Venâncio Silva, S. & de Oliveira, M.T. (1997) Raman microspectroscopy of some iron oxides and oxyhydroxides. *Journal of Raman Spectroscopy*, **28**, 873–878.

Felmy, A.R., Cho, H., Rustad, J.R. & Mason, M.J. (2001) An aqueous thermodynamic model for polymerized silica species to high ionic strength. *Journal of Solution Chemistry*, **30**, 509–525.

Francisco, P.C.M., Mitsui, S., Ishidera, T., Tachi, Y., Doi, R. & Shiwaku, H. (2020) Interaction of FeII and Si under anoxic and reducing conditions: Structural characteristics of ferrous silicate co-precipitates. *Geochimica et Cosmochimica Acta*, **270**, 1–20.

Frank-Kamenetzkij, V.A., Kotov, N. V & Tomashenko, A.N. (1973) The role of AlIV and AlVI in transformation and synthesis of layer silicates. *Kristall und Technik*, **8**, 425–435.

Galai, L., Marchetti, L., Miserque, F., Frugier, P., Godon, N., Brackx, E., Remazeilles, C. & Refait, P. (2023) Effect of dissolved Si on the corrosion of iron in deaerated and slightly alkaline solutions (pH ≈ 8.1) at 50 °C. *Corrosion Science*, **210**, 110790.

https://doi.org/10.1180/clm.2024.8 Published online by Cambridge University Press

Gong, K., Aytas, T., Zhang, S.Y. & Olivetti, E.A. (2022) Data-Driven Prediction of Quartz Dissolution Rates at Near-Neutral and Alkaline Environments. *Frontiers in Materials*, **9**, 1–15.

Grubb, P.L.C. (1971) Silicates and their paragenesis in the brockman iron formation of Wittenoom Gorge, Western Australia. *Economic Geology*, **66**, 281–292.

Gunnarsson, I. & Arnórsson, S. (2000) Amorphous silica solubility and the thermodynamic properties of H4SiO°4 in the range of 0° to 350°C at Psat. *Geochimica et Cosmochimica Acta*, **64**, 2295–2307.

Halevy, I., Alesker, M., Schuster, E.M., Popovitz-Biro, R. & Feldman, Y. (2017) A key role for green rust in the Precambrian oceans and the genesis of iron formations. *Nature Geoscience*, **10**, 135–139.

Harder, H. (1978) Synthesis of Iron Layer Silicate Minerals. *Clays and Clay Minerals*, **26**, 65–72.

Herbert, H.-J., Kasbohm, J., Nguyen-Thanh, L., Meyer, L., Hoang-Minh, T., Xie, M. & Mählmann, R.F. (2016) Alteration of expandable clays by reaction with iron while being percolated by high brine solutions. *Applied Clay Science*, **121–122**, 174–187.

Hinz, I.L., Nims, C., Theuer, S., Templeton, A.S. & Johnson, J.E. (2021) Ferric iron triggers greenalite formation in simulated Archean seawater. *Geology*, **49**, 905–910.

Jaber, M., Komarneni, S. & Zhou, C.-H. (2013) Synthesis of Clay Minerals. Pp. 223–241 in: *Handbook of Clay Science Fundamentals* (F. Bergaya & G. Lagaly, editors). Elsevier.

Kikuchi, R., Sato, T., Fujii, N., Shimbashi, M. & Arcilla, C.A. (2022) Natural glass alteration under a hyperalkaline condition for about 4000 years. *Scientific Reports*, **12**, 1–10.

Kilaas, R. (1998) Optimal and near-optimal filters in high-resolution electron microscopy. *Journal of Microscopy*, **190**, 45–51.

de Kimpe, C., Gastuche, M.C. & Brindley, G.. (1961) Ionic coordination in alumino-silicic gels in relation to clay mineral formation. *American Mineralogist*, **46**, 1370–1381.

Kloprogge, J.T. (1994) Solid-State Nuclear Magnetic Resonance Spectroscopy on Synthetic Ammonium/Aluminum-Saponites*. *Clays and Clay Minerals*, **42**, 416–420.

Kloprogge, J.T. (1998) Synthesis of smectites and porous pillared clay catalysts: a review. *Journal of Porous Materials*, **5**, 5–41.

Konhauser, K.O., Amskold, L., Lalonde, S. V., Posth, N.R., Kappler, A. & Anbar, A. (2007) Decoupling photochemical Fe(II) oxidation from shallow-water BIF deposition. *Earth and Planetary Science Letters*, **258**, 87–100.

Lanson, B., Lantenois, S., van Aken, P.A., Bauer, A. & Plancon, A. (2012) Experimental

https://doi.org/10.1180/clm.2024.8 Published online by Cambridge University Press

investigation of smectite interaction with metal iron at 80 C: Structural characterization of newly formed Fe-rich phyllosilicates. *American Mineralogist*, **97**, 864–871.

Lantenois, S., Lanson, B., Muller, F., Bauer, A., Jullien, M. & Plançon, A. (2005) Experimental study of smectite interaction with metal Fe at low temperature: 1. Smectite destabilization. *Clays and Clay Minerals*, **53**, 597–612.

Manceau, A. (1995) Crystal Chemistry of Hydrous Iron Silicate Scale Deposits at the Salton Sea Geothermal Field. *Clays and Clay Minerals*, **43**, 304–317.

Marks, L.D. (1996) Wiener-filter enhancement of noisy HREM images. *Ultramicroscopy*, **62**, 43–52.

Meite, F., Hauet, T., Billard, P., Ferté, T., Abdelmoula, M. & Zegeye, A. (2022) Insight into the magnetic properties of Pb-dopped iron oxide nanoparticles during Fe(III) bio-reduction by Shewanella oneidensis MR-1. *Chemical Geology*, **606**, 120904.

Mizutani, T., Fukushima, Y., Okada, A., Kamigaito, O. & Kobayashi, T. (1991) Synthesis of 1:1 and 2:1 Iron Phyllosilicates and Characterization of their Iron State by Mössbauer Spectroscopy. *Clays and Clay Minerals*, **39**, 381–386.

Mosser-Ruck, R., Cathelineau, M., Guillaume, D., Charpentier, D., Rousset, D., Barres, O. & Michau, N. (2010) Effects of Temperature, pH, and Iron/Clay and Liquid/Clay Ratios on Experimental Conversion of Dioctahedral Smectite to Berthierine, Chlorite, Vermiculite, or Saponite. *Clays and Clay Minerals*, **58**, 280–291.

Murad, E. & Johnston, J.H. (1987) Iron oxides and oxyhydroxides. Pp. 507–582 in: *Mössbauer Spectroscopy Applied to Inorganic Chemistry Volume 2* (G.J Long, editor). Springer New York, NY.

Petit, S., Baron, F. & Decarreau, A. (2017) Synthesis of nontronite and other Fe-rich smectites : a critical review. *Clay Minerals*, **52**, 469–483.

Pignatelli, I., Bourdelle, F., Bartier, D., Mosser-Ruck, R., Truche, L., Mugnaioli, E. & Michau, N. (2014) Iron–clay interactions: Detailed study of the mineralogical transformation of claystone with emphasis on the formation of iron-rich T–O phyllosilicates in a step-by-step cooling experiment from 90 °C to 40 °C. *Chemical Geology*, **387**, 1–11.

Rancourt, D.G. & Ping, J.Y. (1991) Voigt-based methods for arbitrary-shape static hyperfine parameter distributions in Mössbauer spectroscopy. *Nuclear Instruments and Methods in Physics Research Section B: Beam Interactions with Materials and Atoms*, **58**, 85–97.

Schwertmann, U. & Cornell, R.M. (eds.). (2000) *Iron Oxides in the Laboratary*. P. in.: Wiley-VCH Verlag GmbH, Weinheim, Germany.

Schwertmann, U. & Thalmann, H. (1976) The Influence of [Fe(II)], [Si], and pH on the

https://doi.org/10.1180/clm.2024.8 Published online by Cambridge University Press

formation of lepidocrocite and ferrihydrite during oxidation of aqueous FeCl2 solutions. *Clay Minerals*, **11**, 189–200.

Stucki, J.W., Goodman, B.A. & Schwertmann, U. (eds.). (1989) *Iron in Soils and Clay Minerals*. P. in: *Soil Science*. D. Reidel Publishing Company, 310 pp.

Tosca, N.J., Guggenheim, S. & Pufahl, P.K. (2016) An authigenic origin for Precambrian greenalite: Implications for iron formation and the chemistry of ancient seawater. *Geological Society of America Bulletin*, **128**, 511–530.

Vandenberghe, R.E., Barrero, C.A., da Costa, G.M., Van San, E. & De Grave, E. (2000) Mössbauer characterization of iron oxides and (oxy)hydroxides: the present state of the art. *Hyperfine Interactions*, **126**, 247–259.

https://doi.org/10.1180/clm.2024.8 Published online by Cambridge University Press